Photophysics of SBFO: A Fluorescent Indicator for Na^+

Katrien Meuwis,[†] Noël Boens,*[,†] Frans C. De Schryver,[†] Marcel Ameloot,[‡] Jacques Gallay,[§] and Michel Vincent[§]

Department of Chemistry, Katholieke Universiteit Leuven, 3001 Heverlee, Belgium, Limburgs Universitair Centrum, 3590 Diepenbeek, Belgium, and Laboratoire pour l'Utilisation du Rayonnement Electromagnétique, Centre Universitaire Paris-Sud, 91405 Orsay, France

Received: July 8, 1997; In Final Form: October 21, 1997[⊗]

SBFO is a commercially available fluorescent indicator for the determination of Na^+ concentrations. To investigate the reversible reaction of Na^+ with this indicator in the ground and excited states, steady-state and time-resolved fluorescence measurements were performed. Global compartmental analysis was used to describe the fluorescence decay surfaces yielding the following values for the rate constants at room temperature in aqueous solution at pH 7.2: $k_{01} = 5 \times 10^8$ s^{-1}, 2×10^7 M^{-1} s^{-1} < k_{21} < 3×10^8 M^{-1} s^{-1}, $k_{02} = 5 \times 10^8$ s^{-1}, $k_{12} = 1 \times 10^8$ s^{-1}. k_{01} and k_{02} denote the respective deactivation rate constants of the Na^+ free and bound forms of the indicator in the excited state. k_{21} represents the second-order rate constant of association of Na^+ with SBFO in the excited state, whereas k_{12} is the first-order rate constant of dissociation of the excited Na^+−indicator complex. The effect of the reversible excited-state reaction between Na^+ and the indicator on the fluorimetric determination of K_d can be neglected.

1. Introduction

The design and applications of fluorescent indicators for the nondestructive determination of intracellular Ca^{2+}, Na^+, K^+, and Mg^{2+} concentrations and of intracellular pH are the subject of intensive research.[1] SBFO is a commercially available fluorescent indicator for the real-time determination of Na^+ concentrations. This sodium indicator consists of a diazacrown ether linked via its nitrogens to a benzofuran oxazole (Figure 1). The cavity size of the complex-forming group confers selectivity for Na^+.

At pH 7, the molar extinction coefficient of SBFO in the absence of Na^+ is approximately 25000 M^{-1} cm^{-1} at 355 nm.[2] The ground-state dissociation constant K_d of the Na^+−SBFO complex is 95 mM in the presence of physiological concentrations of K^+ and 50 mM without K^+.[2] SBFO binds Na^+ with a 1:1 stoichiometry, inducing a 3-fold enhancement in fluorescence intensity and shifting the maxima of the excitation and emission spectra to shorter wavelengths. The fluorescence is relatively unaffected by changes in pH between 6.5 and 7.5. The measurements leading to the determination of the ground-state dissociation constant K_d of the formed complex are often performed by fluorimetry. However, fluorescence depends on both ground-state and excited-state parameters. It is not generally acknowledged that the binding reaction of the ion to the indicator in the excited state and the corresponding dissociation of the formed complex may influence the value of K_d derived from a fluorimetric titration. The degree of interference of the excited-state reaction with the fluorimetric determination of K_d depends on the values of the excited-state rate constants and/or the chosen excitation and emission wavelengths.[3] These values can be assessed by the one-step global compartmental analysis[4,5] of the fluorescence decay surfaces of an indicator as a function of the ion concentration.

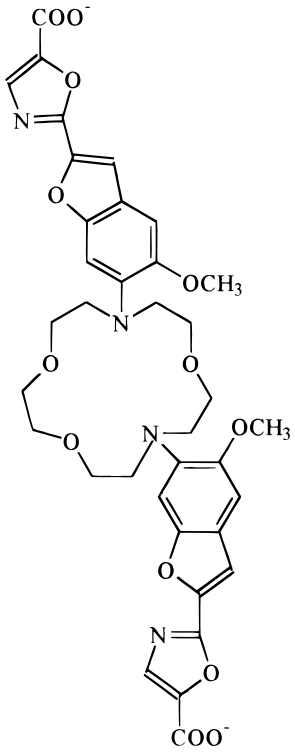

Figure 1. Chemical structure of SBFO.

In this paper, values of the four rate constants defining the excited-state reaction are estimated by global compartmental analysis. The estimated rate constant values enable one to investigate the influence of the excited-state reaction on the fluorimetric determination of K_d.

* To whom correspondence should be addressed. Tel.: +-32-(0)16-327497. Fax: +-32-(0)16-327990. E-mail: Noel.Boens@chem.kuleuven.ac.be.
[†] Katholieke Universiteit Leuven.
[‡] Limburgs Universitair Centrum.
[§] Centre Universitaire Paris-Sud.
[⊗] Abstract published in *Advance ACS Abstracts,* December 15, 1997.

S1089-5647(97)02224-4 CCC: $15.00
Published on Web 01/15/1998

SCHEME 1

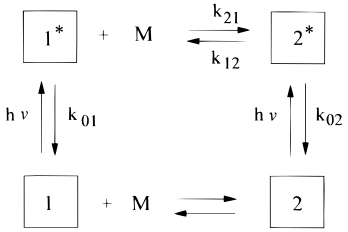

2. Theory

2.1. Kinetics. Consider a causal, linear, time-invariant, intermolecular system consisting of two distinct types of ground-state species and two corresponding excited-state species as is depicted in Scheme 1. Ground-state species **1** can reversibly react with M to form ground-state species **2**. For SBFO, **1** represents the ground state of the free form of the indicator, **2** is the ground state of the Na^+-SBFO complex, and M denotes Na^+. Excitation by light creates the excited-state species **1*** and **2***, which can decay by fluorescence (F) and nonradiative (NR) processes. The composite rate constant for these processes is denoted by k_{0i} ($=k_{Fi} + k_{NRi}$) for species **i***. The second-order rate constant describing the association **1*** + M → **2*** is represented by k_{21}. The first-order rate constant for the dissociation of **2*** into **1*** and M is denoted by k_{12}.

If the system depicted in Scheme 1 is excited by a δ-pulse that does not significantly alter the concentrations of the ground-state species, the fluorescence δ-response function, $f(\lambda^{ex},\lambda^{em},t)$, measured at emission wavelength λ^{em} due to excitation at λ^{ex} is expressed by[4]

$$f(\lambda^{ex},\lambda^{cm},t) = \kappa\tilde{\mathbf{c}}(\lambda^{em})\,\mathbf{U}\exp(t\Gamma)\,\mathbf{U}^{-1}\,\tilde{\mathbf{b}}(\lambda^{ex}), \quad t \geq 0 \quad (1)$$

with κ a proportionality constant. $\mathbf{U} = [\mathbf{U_1},\mathbf{U_2}]$ is the matrix of the two eigenvectors of matrix **A** (eq 2) and $\mathbf{U}^{-1}$ the inverse of **U**. γ_1 and γ_2 are the eigenvalues of **A** corresponding to $\mathbf{U_1}$ and $\mathbf{U_2}$, and $\exp(t\Gamma) = \mathrm{diag}\{\exp(\gamma_1 t),\exp(\lambda_2 t)\}$.

$$\mathbf{A} \equiv \begin{bmatrix} -(k_{01} + k_{21}[\mathrm{M}]) & k_{12} \\ k_{21}[\mathrm{M}] & -(k_{02} + k_{12}) \end{bmatrix} \quad (2)$$

$\tilde{\mathbf{b}}(\lambda^{ex})$ is the 2×1 vector with elements $\tilde{b}_i(\lambda^{ex})$ defined by

$$\tilde{b}_i = b_i/(b_1 + b_2) \quad (3)$$

where b_i denotes the concentration of **i*** at time zero:

$$b_i = [\mathbf{i}^*]_{t=0} \quad (4)$$

which, in the low excitation limit and when Beer's law is valid, is proportional to the ground-state absorbance of **i**. Hence, in the low excitation limit and when Beer's law is valid (as in single-photon timing experiments),[6,7] $\tilde{b}_i$ represents the normalized absorbance of species **i** at λ^{ex}. The elements b_i (and $\tilde{b}_i$) depend on [M].

$\tilde{\mathbf{c}}(\lambda^{em})$ is the 1×2 vector of the normalized emission weighting factors $\tilde{c}_i(\lambda^{em})$ of species **i*** at λ^{em}:

$$\tilde{c}_i = c_i/(c_1 + c_2) \quad (5)$$

The emission weighting factors $c_i(\lambda^{em})$ are given by

$$c_i(\lambda^{em}) = k_{Fi}\int_{\Delta\lambda^{em}}\rho_i(\lambda^{em})\,\mathrm{d}\lambda^{em} \quad (6)$$

k_{Fi} represents the fluorescence rate constant of species **i***; $\Delta\lambda^{em}$ is the emission wavelength interval around λ^{em} where the fluorescence signal is monitored; $\rho_i(\lambda^{em})$ is the emission density of **i*** at emission wavelength λ^{em}, normalized to the complete steady-state fluorescence spectrum F_i of **i***. $\rho_i(\lambda^{em})$ is defined by

$$\rho_i(\lambda^{em}) = F_i(\lambda^{em})/\int_{\text{full band}} F_i\,\mathrm{d}\lambda^{em} \quad (7)$$

Equation 1 can be written in the common biexponential format:

$$f(\lambda^{ex},\lambda^{em},t) = \alpha_1\exp(\gamma_1 t) + \alpha_2\exp(\gamma_2 t), \quad t \geq 0 \quad (8)$$

The exponential factors $\gamma_{1,2}$ are related to the decay times $\tau_{1,2}$ according to

$$\gamma_{1,2} = -1/\tau_{1,2} \quad (9)$$

and are given by

$$\gamma_{1,2} = -{}^1/_2\{S_1 + S_2 \mp [(S_1 - S_2)^2 + 4k_{21}k_{12}[\mathrm{M}]]^{1/2}\} \quad (10)$$

with

$$S_1 = k_{01} + k_{21}[\mathrm{M}] \quad (11a)$$

$$S_2 = k_{02} + k_{12} \quad (11b)$$

For clarity, we shall not use the notation $\tau_{1,2}$ (and $\alpha_{1,2}$), but we shall refer to τ_L (and corresponding α_L, L for long) and τ_S (and corresponding α_S, S for short).

2.2. Fluorimetric Titration. If the system depicted in Scheme 1 is excited with light of constant intensity, and if the absorbance of the sample is less than 0.1, the measured steady-state fluorescence signal $F(\lambda^{ex},\lambda^{em},[\mathrm{M}])$ observed at λ^{em} due to excitation at λ^{ex} is given by[3]

$$F(\lambda^{ex},\lambda^{em},[\mathrm{M}]) = \frac{\epsilon_1(\lambda^{ex})\,a_1(\lambda^{em},[\mathrm{M}])K_d + \epsilon_2(\lambda^{ex})\,a_2(\lambda^{em},[\mathrm{M}])[\mathrm{M}]}{K_d + [\mathrm{M}]} C_T\psi(\lambda^{ex},\lambda^{em}) \quad (12)$$

where $\epsilon_i(\lambda^{ex})$ represents the molar extinction coefficient of species **i** at λ^{ex}. The coefficients a_i are given by[3,8]

$$a_1(\lambda^{em},[\mathrm{M}]) = \frac{(k_{02} + k_{12})c_1(\lambda^{em}) + k_{21}[\mathrm{M}]c_2(\lambda^{em})}{k_{01}(k_{02} + k_{12}) + k_{02}k_{21}[\mathrm{M}]} \quad (13a)$$

$$a_2(\lambda^{em},[\mathrm{M}]) = \frac{k_{12}c_1(\lambda^{em}) + (k_{01} + k_{21}[\mathrm{M}])c_2(\lambda^{em})}{k_{01}(k_{02} + k_{12}) + k_{02}k_{21}[\mathrm{M}]} \quad (13b)$$

The factor $\psi(\lambda^{ex},\lambda^{em})$ includes instrumental parameters,

$$\psi(\lambda^{ex},\lambda^{em}) = 2.3dI_0(\lambda^{ex})\,\xi(\lambda^{em}) \quad (14)$$

where d denotes the excitation light path length, $I_0(\lambda^{ex})$ represents the intensity of the exciting light at λ^{ex} impinging on the sample, and $\xi(\lambda^{em})$ is a factor taking into account the efficiency of both the optics and the detector. The ground-state dissociation constant, K_d, and the total analytical concentration, C_T, of the fluorescent indicator are given by eqs 15 and 16, respectively.

$$K_d = [\mathbf{1}][M]/[\mathbf{2}] \quad (15)$$

$$C_T = [\mathbf{1}] + [\mathbf{2}] \quad (16)$$

If $k_{21}[M]$ describing the association of **1*** with M is negligible within the range of used M concentrations, the coefficients a_i become practically independent of [M]. In the limiting case when $k_{21} = 0$, both coefficients $a_{1,2}$ are completely independent of [M] and are given by

$$a_1(\lambda^{em}) = \frac{c_1(\lambda^{em})}{k_{01}} \quad (17a)$$

$$a_2(\lambda^{em}) = \frac{k_{12}c_1(\lambda^{em}) + k_{01}c_2(\lambda^{em})}{k_{01}(k_{02} + k_{12})} \quad (17b)$$

In such a case the fluorescence signal $F(\lambda^{ex},\lambda^{em},[M])$ plotted vs -log[M] shows a unique inflection at -log[M] = pK_d. Therefore, as long as $k_{21}[M] \approx 0$, the excited-state reaction does not interfere with the correct determination of K_d from fluorimetric titration. When the coefficients $a_{1,2}$ are independent of [M], it can be derived from eq 10 that the decay times $\tau_{1,2}$ are independent also of [M].[9] If an inflection occurs in the [M] range of the fluorimetric titration curve F vs -log[M] where the decay times are invariant, this inflection point can be correctly associated with pK_d. In contrast, the inflection point(s) in the [M] range where the decay times vary cannot be attributed to ground-state dissociation.[10]

3. Experimental Methods

3.1. Materials. SBFO diammonium salt was obtained from Molecular Probes (Eugene, OR). MOPS (3-(*N*-morpholino)-propanesulfonic acid) free acid was purchased from SIGMA Chemie (Bornem, Belgium), and NaCl from Aldrich Chimica (Geel, Belgium). All products were used as received. Fluorimetric measurements were performed using aqueous buffer solutions of SBFO in the presence of NaCl. All measurements were done at room temperature. Solutions of NaOH and MOPS were used to obtain the physiological pH value of 7.2. The added Na^+ ions were taken into account in the final calculation of $[Na^+]$. Milli-Q water was used to prepare the aqueous solutions according to the procedure described by Minta and Tsien.[2] The ionic strength of solutions with different $[Na^+]$ was not kept constant.

3.2. Instrumentation. Fully corrected steady-state excitation and emission spectra were recorded on a SPEX Fluorolog 212.

The fluorescence decay traces were collected by the single-photon timing technique[6,7] using the synchrotron radiation facility SUPER-ACO (Anneau de Collision d'Orsay at LURE, France) as described elsewhere.[11] The storage ring provided vertically polarized light pulses with a full width at half-maximum of ≈500 ps at a frequency of 8.33 MHz in double bunch mode. A Hamamatsu microchannel plate R1564U-06 was utilized to detect the fluorescence photons under magic angle (54°44′). The instrument response function was determined by measuring the light scattered by glycogen in aqueous solution at the emission wavelength. All decay traces were collected in 1K channels of a multichannel analyzer and contained about 5000 peak counts. The time increment per channel was 21.4 ps.

3.3. Data Analysis. The global compartmental analysis of the fluorescence decay surface of species undergoing excited-state processes was implemented in the existing general global analysis program[12] based on Marquardt's[13] algorithm.

The fitting parameters were determined by minimizing the global reduced chi-square χ_g^2:

$$\chi_g^2 = \sum_l^q \sum_i w_{li}(\gamma_{li}^o - \gamma_{li}^c)^2/\nu \quad (18)$$

where the index l sums over q experiments, and the index i sums over the appropriate channel limits for each individual experiment. γ_{li}^o and γ_{li}^c denote, respectively, the experimentally measured (observed) and fitted (calculated) values corresponding to the ith channel of the lth experiment. w_{li} is the corresponding statistical weight. ν represents the number of degrees of freedom for the entire multidimensional fluorescence decay surface. The statistical criteria to judge the quality of the fit comprised both graphical and numerical tests. The graphical methods included plots of the surfaces (carpets) of the autocorrelation function values vs experiment number and of the weighted residuals vs channel number. χ_g^2 and its corresponding $Z_{\chi_g^2}$ (eq 19) provide numerical goodness-of-fit criteria for the entire fluorescence decay surface.

$$Z_{\chi_g^2} = (\chi_g^2 - 1)(\nu/2)^{1/2} \quad (19)$$

Using $Z_{\chi_g^2}$, the goodness-of-fit of analyses with different ν can be readily compared. The additional criteria to judge the quality of the fits are described elsewhere.[7] Standard error estimates were obtained from the parameter covariance matrix available from the nonlinear least-squares analysis. All quoted errors are one standard deviation. All simulations and analyses were done on an IBM RISC System/6000 computer.

3.4. Synthetic Data Generation. To test the validity of the conclusions, computer-generated decay data were used. Synthetic biexponential fluorescence decay traces as a function of [M] were generated as described before.[14] All computer-simulated decays had 1K data points with a different number of counts (5000, 10 000, 20 000, 100 000) in the peak channel. In the data generation different emission wavelengths were mimicked by the use of different values of $\tilde{c}_1$. $\tilde{b}_1$ values were computed using experimental values of SBFO for ϵ_1, ϵ_2, K_d, and [M].

4. Results

The ground-state dissociation constant K_d of the Na^+−SBFO complex was determined from a Hill plot using fluorescence measurements at 20 °C, pH 7.2 in aqueous solution in the absence of K^+. The linear Hill plot (with correlation coefficient 0.998, Figure 2) yielded a value of 34 mM for K_d (pK_d = 1.47 ± 0.05) and indicated a 1:1 stoichiometry for the Na^+−SBFO complex. The pK_d value is in reasonable correspondence with the value estimated by Minta and Tsien (pK_d = 1.30).[2]

The molar extinction coefficients at 340 and 355 nm were determined at four different SBFO concentrations in the absence (ϵ_1) and in the presence of 270 mM Na^+ (ϵ_2), yielding the following values: ϵ_1 = 42 600 M^{-1} cm^{-1}, ϵ_2 = 42 100 M^{-1} cm^{-1} at 340 nm; ϵ_1 = 50 000 M^{-1} cm^{-1}, ϵ_2 = 36 400 M^{-1} cm^{-1} at 355 nm.

Decay traces of SBFO at different $[Na^+]$ ranging from 2.68 mM to 3.07 M were measured at three different sets of excitation/emission wavelengths: (i) λ^{ex} = 340 nm, λ^{em} = 500 nm; (ii) λ^{ex} = 340 nm, λ^{em} = 510 nm; (iii) λ^{ex} = 355 nm, λ^{em} = 510 nm.

The decay traces of solutions with identical Na^+ concentrations were analyzed globally as biexponential functions with the decay times linked over the emission and excitation

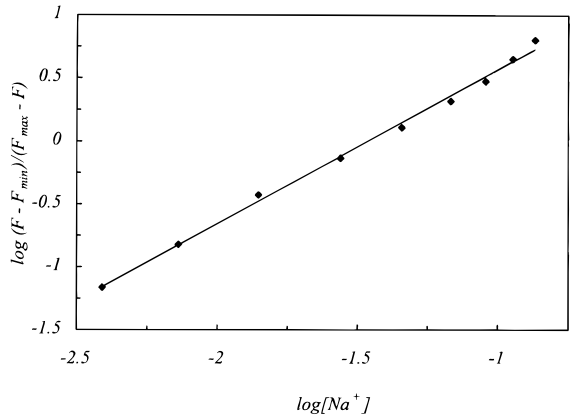

Figure 2. Hill plot constructed with the steady-state fluorescence signals F(340 nm,500 nm) of SBFO vs log[Na^+] at pH 7.2 in aqueous K^+ free solution at room temperature.

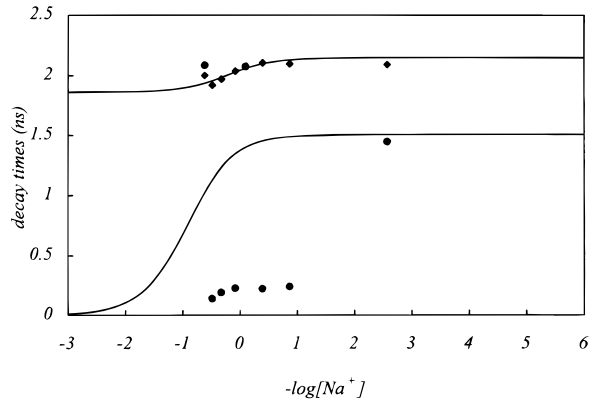

Figure 3. Decay times (—) of SBFO as a function of -log[Na^+] calculated according to eqs 9−11 using the rate constant values obtained from global compartmental analysis (Table 1). The symbols ◆ and ● represent τ_L and τ_S, respectively, estimated by global biexponential analysis at each [Na^+].

wavelengths at each [Na^+]. Biexponential analyses gave good fits at each Na^+ concentration. The recovered $\tau_{S,L}$ values are graphically compiled in Figure 3, showing that with increasing [Na^+] τ_L decreases, indicating that $k_{01} < k_{02}$.[9] The variation of τ_S as a function of -log[Na^+] is erratic. This could be due to the negligible values of the preexponential values associated with the short decay times. It was shown[15] that global biexponential analysis fails to give accurate and precise estimates of the short decay time τ_S when decays traces are combined of which the contribution of τ_S to the total fluorescence is small. Furthermore, global biexponential analysis of decay traces with nearly invariant contributions of the decay components results in poor estimates of the decay times.[15] Indeed, varying the excitation and emission wavelengths as done experimentally in the collection of the decays hardly changes the preexponential factors (see further). The statement that τ_L at [Na^+] → 0 is associated with k_{01} should be substantiated by the decrease with decreasing [Na^+] of the ratio α_S/α_L at $\lambda^{ex} = 340$ nm and $\lambda^{em} = 500$ nm estimated by the simultaneous biexponential analyses.[9] However, the variation of this amplitude ratio is not as expected. Apparently global biexponential analysis could accurately recover only the long decay time and not the short decay time nor the corresponding amplitudes.

In global compartmental analysis all (46) decay traces were simultaneously analyzed. The resulting rate constant values are shown in Table 1. Using these rate constant values, the decay times were calculated as a function of [Na^+] according to eqs 9−11. These decay times are shown graphically in Figure 3

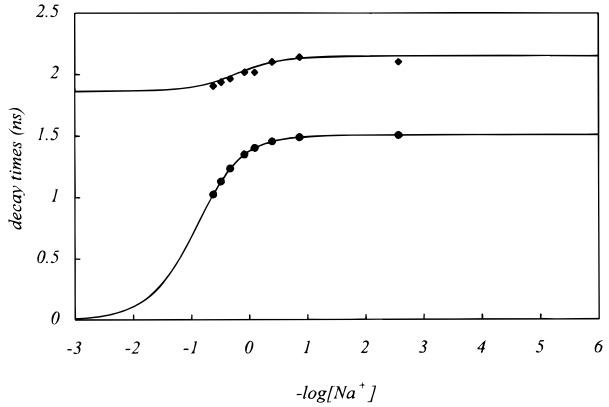

Figure 4. Decay times (—) of SBFO as a function of -log[Na^+] calculated according to eqs 9−11 using the rate constant values obtained from global compartmental analysis (Table 1). The symbols ◆ represent τ_L estimated by global biexponential analysis in which τ_S (●) was held fixed at the value calculated according to eqs 9−11 using the rate constant values of Table 1.

TABLE 1: Rate Constant Values (±Standard Deviation) of SBFO Estimated by Global Compartmental Analysis

rate constant	
k_{01} $(ns)^{-1}$	0.465 (±0.001)
k_{21} $(M\ ns)^{-1}$	0.087 (±0.004)
k_{02} $(ns)^{-1}$	0.537 (±0.002)
k_{12} $(ns)^{-1}$	0.127 (±0.002)

as a function of -log[Na^+] together with the decay times estimated directly from global biexponential analysis. It is clear that for τ_L there is a good agreement between these two sets of decay times. The agreement between the τ_S values is, however, not satisfactory. From global compartmental analysis, it is also possible to determine the values of the normalized absorbances of each species at time zero. These $\tilde{b}_1$ values estimated by global compartmental analysis are not in good agreement with the ones calculated on the basis of the molar extinction coefficients ϵ_1 and ϵ_2, K_d, and [Na^+].

The global biexponential analysis with τ_L freely adjustable and with τ_S held fixed at the value calculated according to eqs 9−11 using the rate constant values of Table 1 yields the decay time values plotted in Figure 4. The agreement between the τ_L values estimated by this global biexponential analysis and those computed according to eqs 9−11 using the rate constant values of Table 1 is excellent.

It is obvious that there are problems with the accuracy of the parameter recovery from the simultaneous analyses (global biexponential as well as compartmental) which merit further investigation. To gain deeper insight into the reasons of the failure to recover reliable parameter estimates, we generated fluorescence decay traces by computer using the values of the rate constants obtained by global compartmental analysis (see Table 1). The values of $\tilde{c}_1$ are those obtained by global compartmental analysis: $\tilde{c}_1 = 0.309$ at 500 nm and $\tilde{c}_1 = 0.289$ at 510 nm. The $\tilde{b}_1$ values were computed using the values of ϵ_1 and ϵ_2 at 340 nm and 355 nm, and $K_d = 34$ mM. The eight values of [M] are the experimentally used Na^+ concentrations. At each [M], three fluorescence decay curves were simulated mimicking the experimental excitation/emission combinations: (i) $\lambda^{ex} = 340$ nm, $\lambda^{em} = 500$ nm; (ii) $\lambda^{ex} = 340$ nm, $\lambda^{em} = 510$ nm; (iii) $\lambda^{ex} = 355$ nm, $\lambda^{em} = 510$ nm. The number of counts in the peak channel was approximately 5000, mimicking the experimental situation. Figure 5 shows the simulated decay times $\tau_{S,L}$ and their corresponding amplitudes $\alpha_{S,L}$ as a function

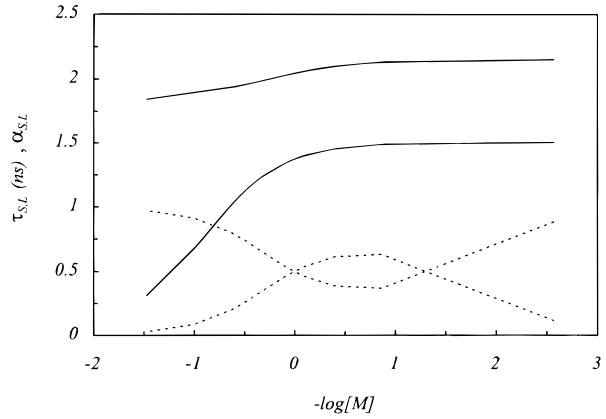

Figure 5. Preexponentials $\alpha_{S,L}$ (···) and decay times $\tau_{S,L}$ (—) as a function of -log[M] calculated with the rate constants of Table 1. See text for details.

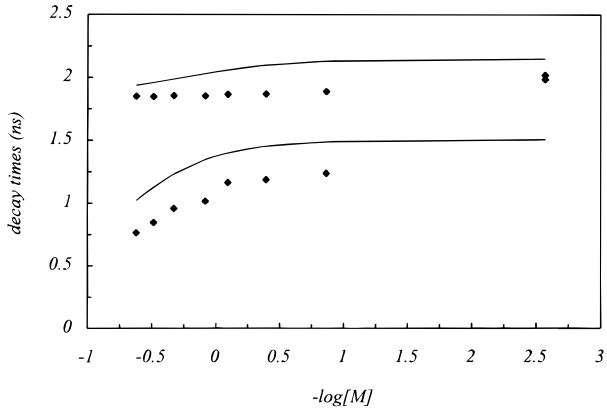

Figure 6. Symbols ◆ represent τ_L and τ_S as a function of -log[M] estimated by global biexponential analysis of the simulated decay traces with 5000 counts in the peak channel. τ_L and τ_S as a function of -log[M] calculated according to eqs 9−11 using the rate constant values of Table 1 are represented by solid lines.

of [M]. It is clear that when τ_S decreases with higher [M], the value of α_S drops to zero.

In a first step, the simulated decay curves at each [M] were analyzed simultaneously as biexponentials. Global biexponential analysis gave good fits at each [M]. Figure 6 shows the estimated decay times $\tau_{S,L}$ as a function of -log[M]. The failure of the global biexponential analyses in obtaining accurate estimates for the decay times is obvious. Additionally, the recovered values of the amplitudes (not shown) were unacceptable.

In a second step, all 24 decay traces at all [M] were analyzed together using global compartmental analysis. The estimated rate constants are compiled in Table 2, which indicates that acceptable estimates are obtained only for k_{01} and the sum (k_{02} + k_{12}). The value of k_{21} was not estimated accurately.

Earlier work[9] has shown that an accurate and precise recovery of the rate constants, and especially of k_{21}, is only possible for analyses of fluorescence decays in the region where the decay times vary, i.e. for SBFO in the [M] range where -log[M] = +1 to −2. Therefore, one might assume that the unsatisfactory recovery of k_{21} is due to the limited [M] range (and hence τ values) employed in the simulations. To check this hypothesis, additional fluorescence decays were simulated at two higher [M]—although not realistic [Na^+]—namely 10 and 30 M. The resulting decay surfaces were then analyzed using global biexponential and compartmental analyses. No improvement in the parameter recovery was observed. Apparently, the rate constants can only be accurately estimated from decay traces collected at [M] where $\tau_{S,L}$ vary, provided that the corresponding $\alpha_{S,L}$ are not negligible.[9] Figure 5 shows that the amplitude α_S vanishes when τ_S decreases at higher [M] so that the extended range of τ_S values is offset by the disappearance of its corresponding amplitude α_S. This accounts for the inaccurate value of k_{21}.

Up to now, nothing has been said about the signal-to-noise ratio of the experiments and the mimicked simulated decay data. Indeed, all decays were experimentally collected (and simulated) with about 5000 counts in the peak channel. Now we will investigate the influence of the number of counts (i.e., the signal-to-noise ratio) on the accuracy of the estimated system parameters. Therefore, we simulated three additional fluorescence decay surfaces in which the constituting traces all had either 10 000, 20 000, or 100 000 counts in the peak channel. Except for the scaling factors, all the simulation parameters were the same as in the simulations with 5000 peak counts. The decay curves at each [M] were then analyzed as biexponentials. The estimated decay times are compiled in Figure 7a,b for the decays with 20 000 and 100 000 peak counts, respectively. From Figure 7, it is obvious that there is an improvement with higher signal-to-noise ratio of the accuracy of the estimates of the decay times $\tau_{S,L}$. Also the corresponding amplitudes (data not shown) are recovered with higher accuracy when the signal-to-noise ratio increases. The results of the analyses of the decays with 10 000 peak counts are intermediate between those with 5000 (Figure 6) and 20 000 (Figure 7a) peak counts. Subsequently, the 24 decay traces of each fluorescence decay surface were analyzed by global compartmental analysis. For each number of counts in the peak channel, the recovered rate constants and the $\tilde{b}_1$ values are compiled in Tables 2 and 3, respectively. It is evident that the most reliable estimates of the parameters are obtained for the analyses of decays with 100 000 counts in the peak channel. Although the estimates of the rate constants k_{01}, k_{02}, and k_{12} at 100 000 counts are accurate and precise, the $\tilde{b}_1$ values at 100 000 counts are acceptable only at the four lowest [M]. At the higher [M], the values of $\tilde{b}_1$ are too small to be determined accurately. One can conclude that only analyses of decays with 100 000 peak counts give satisfactory results. However, from an experimental point of view, collecting a fluorescence decay surface as a function of excitation and emission wavelengths and [M] with decays containing 100 000 counts in the peak channel is a very time-consuming task (a single decay trace with 100 000 peak counts takes between 10 and 20 h to collect depending on the excitation and emission

TABLE 2: Rate Constant Values (±Standard Deviation) Estimated by Global Compartmental Analysis of Simulated Decays with Different Number of Counts in the Peak Channel. In Each Analysis 24 Decay Traces Were Analyzed Together

		estimated values			
rate constant	true values	5000 counts	10 000 counts	20 000 counts	100 000 counts
k_{01} (ns^{-1})	0.465	0.487 (±0.001)	0.475 (±0.001)	0.470 (±0.001)	0.466 (±0.001)
k_{21} (M^{-1} ns^{-1})	0.087	0.21 (±0.01)	0.158 (±0.006)	0.144 (±0.004)	0.101 (±0.002)
k_{02} (ns^{-1})	0.537	0.552 (±0.001)	0.540 (±0.001)	0.539 (±0.001)	0.537 (±0.001)
k_{12} (ns^{-1})	0.127	0.102 (±0.003)	0.116 (±0.002)	0.116 (±0.001)	0.125 (±0.001)

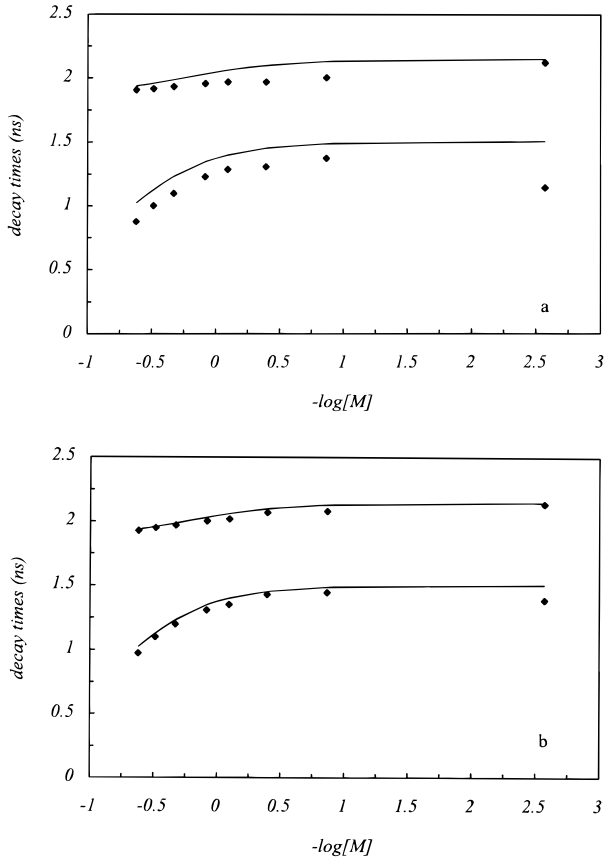

Figure 7. Symbols ◆ represent τ_L and τ_S as a function of -log[M] estimated by global biexponential analysis of the simulated decay traces with (a) 20 000 counts in the peak channel, (b) 100 000 counts in the peak channel. τ_L and τ_S as a function of -log[M] calculated according to eqs 9−11 using the rate constant values of Table 1 are represented by solid lines.

TABLE 3: Values of $\tilde{b}_1$ Estimated by Global Compartmental Analysis of Simulated Decays with a Different Number of Counts in the Peak Channel. In Each Analysis 24 Decay Traces Were Analyzed Together

		estimated $\tilde{b}_1$ values			
[M] (M)	$\tilde{b}_1$[a] true value	5000 counts	10 000 counts	20 000 counts	100 000 counts
0.002 68	0.928	0.982	0.977	0.914	0.934
0.136	0.201	−0.163	0.143	−0.171	0.180
0.404	0.0783	−0.261	−0.004 74	−0.286	0.0553
0.805	0.0409	−0.280	−0.0463	−0.0287	0.0179
1.21	0.0276	−0.256	−0.0601	−0.263	0.0034
2.13	0.0186	−0.227	−0.0623	−0.226	−0.007 26
3.07	0.0111	−0.201	−0.0657	−0.196	−0.009 83
4.18	0.008 42	−0.188	−0.0614	−0.169	−0.0101

[a] $\tilde{b}_1$ at each [M] was calculated using the values of $\epsilon_1 = 42\,600$ M^{-1} cm^{-1}, $\epsilon_2 = 42\,100$ M^{-1} cm^{-1} (at 340 nm), and $K_d = 34$ mM.

wavelengths, the Na^+ concentration, and the time lapsed between the injection in the storage ring and the collection of the decays). Even decays with 20 000 peak counts do not suffice to obtain accurate rate constant estimates. Therefore, at low signal-to-noise the only reliable information available from the experiments is the values of k_{01} and the sum ($k_{02} + k_{12}$). Note that at low [M] (or [Na^+]) τ_L reaches the value of $1/k_{01}$ and τ_S equals $1/(k_{02} + k_{12})$. It is not possible to estimate k_{21} accurately.

To have some idea of the magnitude of k_{21}, we performed a repetitive global compartmental analysis of 46 experimentally collected decays in which k_{21} was kept fixed at a preset value

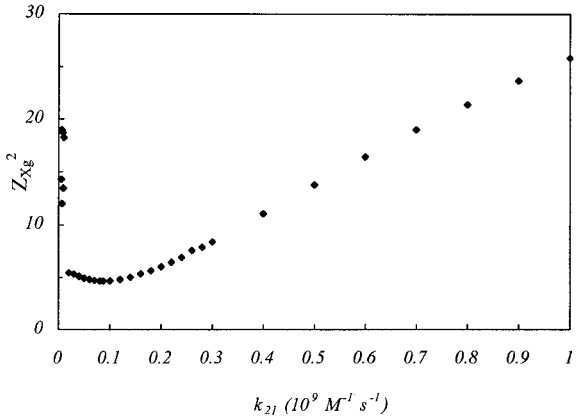

Figure 8. $Z_{\chi_g^2}$ for the global compartmental analyses of the experimental decay curves with fixed values of k_{21}.

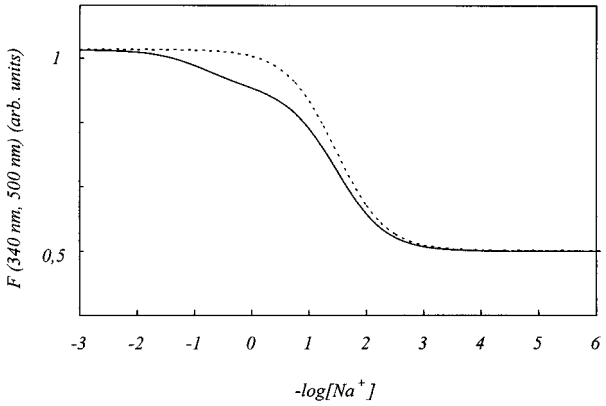

Figure 9. Fluorimetric titration curve F(340 nm,500 nm) computed (—) using the rate constants of Table 1 together with the following experimentally determined values: $K_d = 34$ mM, $\epsilon_1 = 42\,600$ M^{-1} cm^{-1} and $\epsilon_2 = 42\,100$ M^{-1} cm^{-1} at 340 nm, $c_1/c_2 = 0.45$. The dotted line represents the calculated fluorimetric titration curve F assuming that $k_{21} = 0$.

while all other parameters were freely adjustable. The goodness-of-fit parameter $Z_{\chi_g^2}$ for the various analyses as a function of k_{21} is shown in Figure 8. It is evident that acceptable fits are obtained only for a relatively narrow range of k_{21} values (2×10^7 M^{-1} $s^{-1} < k_{21} < 3 \times 10^8$ M^{-1} s^{-1}). The minimum value of $Z_{\chi_g^2}$ was obtained for $k_{21} = 8.7 \times 10^7$ M^{-1} s^{-1}: this value also was recovered by global compartmental analysis with all parameters freely adjustable.

Knowledge of the rate constant values k_{ij}, the dissociation constant K_d, ϵ_1, ϵ_2, and c_1/c_2 allows one to investigate the interference of the excited-state reaction with the fluorimetric determination of K_d. Fluorimetric titration curves were computed with $k_{21} = 0$ and $k_{21} \neq 0$ mimicking excitation at 340 nm and emission at 500 nm. The rate constant values of Table 1 together with experimentally determined values of K_d, ϵ_1, and ϵ_2 at 340 nm and $c_1/c_2 = 0.45$ at 500 nm are used to construct the fluorimetric titration curves F(340 nm,500 nm) vs -log[Na^+] shown in Figure 9. It is evident that the titration curve computed with $k_{21} = 0$ has a single inflection at [Na^+] = 34 mM, corresponding to K_d. The reconstructed titration curve with $k_{21} \neq 0$ exhibits three inflection points at [Na^+] = 0.708, 0.191, and 0.034 M. As both decay times are constant in the region where F vs -log[Na^+] exhibits the inflection point at [Na^+] = 34 mM, this inflection can be attributed to the ground-state dissociation constant K_d.[10] Evidently, the inflections at [Na^+] = 0.191 and 0.708 M are situated in the range where the decay times vary and hence cannot be attributed to K_d.

TABLE 4: Radiative (k_F) and Nonradiative (k_{NR}) Deactivation Rate Constants Values of the Na^+ Free and Bound Forms of SBFO

species	ϕ^a	k_F $(ns)^{-1}$	k_{NR} $(ns)^{-1}$
free form (**1***)	0.14	0.065	0.400
bound from (**2***)	0.44	0.236	0.301

[a] Fluorescence quantum yield values taken from Minta and Tsien.[2]

From the small value of k_{21}, one can predict that K_d can be determined correctly from fluorescence measurements. Indeed, 28 fluorescence decay traces collected in the $[Na^+]$ region from 2.68 mM up to 1.21 M can be analyzed together as biexponentials with linked decay times ($\tau_S = 1.45 \pm 0.01$ ns, $\tau_L = 2.09 \pm 0.01$ ns). The value obtained for pK_d from the Hill plot (Figure 1) occurs in the $[Na^+]$ region where the decay times are invariant, so this value can correctly be associated with pK_d.

Table 4 compiles the rate constant values for fluorescence and nonradiative decay for the Na^+ free and bound forms of SBFO using the values of k_{01}, k_{02}, and the fluorescence quantum yields ϕ. The nonradiative rate constant k_{NR} is comparable for both species, while radiative processes are more important in the bound form (the value of k_F of the Na^+ bound form is about 4 times larger than of the Na^+ free form). This accounts for the increase in fluorescence intensity when the Na^+ concentration is increased.

5. Discussion

It has been shown[16] that global compartmental analysis is a very sensitive method for distinguishing between competing kinetic models. The steady-state (Hill plot) and time-resolved fluorescence (two decay times) data as a function of $[Na^+]$ are compatible with the kinetic model depicted in Scheme 1. The values for the rate constants estimated by global compartmental analysis are physically acceptable. It should be recognized that in a photophysical context a compartment is composed of a distinct type of species which acts kinetically in a unique way. Hence, the time scale of the experimental method defines the nature of the compartment. Upon excitation of the free and bound forms of the fluorescent indicator (**1** and **2**), initially the respective Franck−Condon states of **1*** and **2*** are reached which relax via internal conversion to the respective fluorescent states of **1*** and **2***. The fluorescent state of **1*** may have some charge-transfer character, as was observed in the time-resolved differential spectra of the free ligand of the crowned derivative of the merocyanine dye DCM.[17] Upon excitation of the bound form, the initially formed **2*** may be transformed very rapidly into a loose complex with a weaker binding to the cation followed by a charge-transfer process which leads to the fluorescent state which finally decays to the ground state with rate constant k_{02}.[17] The very fast processes transforming the initially Franck−Condon state to the final fluorescent state can usually not be detected by single-photon timing instrumentation. Picosecond pump−probe spectroscopy can provide evidence for the occurrence of the very fast photodisruption of the interaction between the cation and the nitrogen atoms of the diazacrown owing to intramolecular charge transfer which reduces the electron density of the nitrogen atoms.[17−19] The dissociation constant $K_d^* = k_{12}/k_{21}$ of SBFO in the excited state is at least 1 order of magnitude larger than K_d in the ground state. The fact that the complex is more stable in the ground state than in the excited state was found also for Ca^{2+}−Fura-2,[8] K^+−PBFI,[20] Na^+−SBFI,[10] Li^+−DCM-crown,[17,18] and Ca^{2+}−CM-crown.[17,18]

The excitation and emission spectra of the free ligand and at full complexation are shown in Figure 10. The maximum of

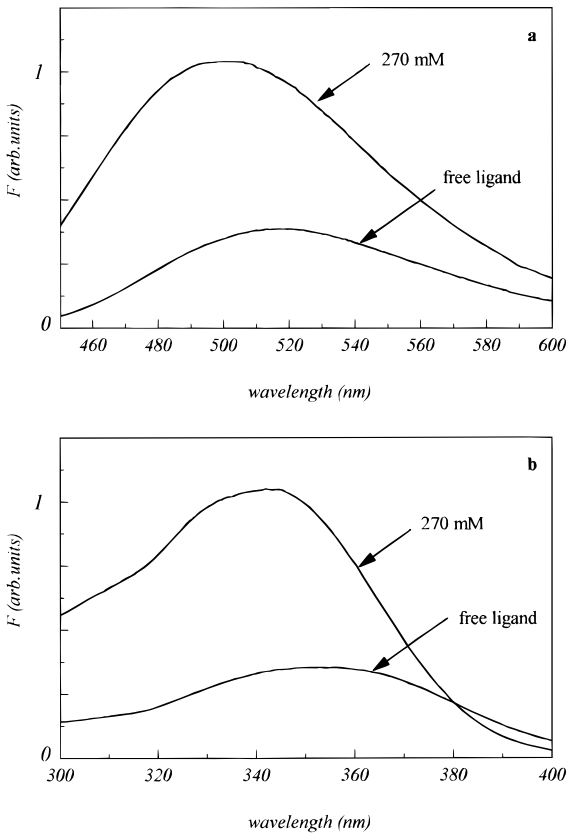

Figure 10. Emission ($\lambda^{ex} = 350$ nm, a) and excitation ($\lambda^{em} = 510$ nm, b) spectra of the free ligand SBFO and at $[Na^+] = 270$ mM (fully complexed) in the presence of MOPS buffer at pH 7.2.

the excitation spectrum of the free ligand ($\lambda^{max} = 353$ nm) shifts to shorter wavelength upon binding Na^+ ($\lambda^{max} = 344$ nm). A comparable hypsochromic shift is observed in the emission spectra: $\lambda^{max} = 520$ nm for the free ligand and $\lambda^{max} = 502$ nm for the fully complexed compound. Consequently, the excitation and emission spectra in the presence of the cation are different from those of the free ligand. These observations do not support a model with photorelease[17,18] of Na^+ from the complex.

6. Conclusions

We have investigated the reversible excited-state reaction between Na^+ and SBFO. Global compartmental analysis was used to estimate the four rate constant values of the excited-state reaction. The value for k_{21} cannot be estimated correctly, but it is possible to specify upper and lower bounds on this rate constant. The effect of the excited-state reaction on the fluorimetric determination of K_d can be neglected.

Acknowledgment. K.M. is a predoctoral fellow of the Vlaams Instituut ter Bevordering van het Wetenschappelijk Technologisch Onderzoek in de Industrie (IWT). N.B. is an Onderzoeksdirecteur of the Fonds voor Wetenschappelijk Onderzoek (FWO). The DWTC is thanked for financial support through IUAP-IV-11.

References and Notes

(1) (a) Czarnik, A. W., Ed. *Fluorescent Chemosensors for Ion and Molecule Recognition*; ACS Symposium Series 538; American Chemical Society: Washington, DC, 1992. (b) Lakowicz, J. R., Ed. *Topics in Fluorescence Spectroscopy; Volume 4: Probe Design and Chemical Sensing*; Plenum Press: New York, 1994. (c) Desvergne, J.-P., Czarnik, A. W., Eds. *Chemosensors for Ion and Molecule Recognition*; NATO ASI Series C 492; Kluwer Academic Publishers: Dordrecht, 1997.

(2) Minta, A.; Tsien R. Y. *J. Biol. Chem.* **1989**, *264*, 19449−19475.
(3) Kowalczyk A.; Boens, N.; Van den Bergh, V.; De Schryver, F. C. *J. Phys. Chem.* **1994**, *98*, 8585−8590.
(4) Ameloot, M.; Boens N.; Andriessen, R.; Van den Bergh, V.; De Schryver, F. C. *J. Phys. Chem.* **1991**, *95*, 2041−2047.
(5) Ameloot, M.; Boens, N.; Andriessen, R.; Van den Bergh, V.; De Schryver, F. C. *Methods Enzymol.* **1992**, *210*, 314−340.
(6) O'Connor, D. V.; Phillips D. *Time-Correlated Single Photon Counting*; Academic Press: London, 1984.
(7) Boens, N. In *Luminescence Techniques in Chemical and Biochemical Analysis*; Baeyens, W. R. G., De Keukeleire, D., Korkidis, K., Eds.; Marcel Dekker: New York, 1991; pp 21−45.
(8) Van den Bergh, V.; Boens, N.; De Schryver, F. C.; Ameloot, M.; Steels, P.; Gallay, J.; Vincent, M.; Kowalczyk, A. *Biophys. J.* **1995**, *68*, 1110−1119.
(9) Van den Bergh, V.; Kowalczyk, A.; Boens, N.; De Schryver, F. C. *J. Phys. Chem.* **1994**, *98*, 9503−9508.
(10) Kowalczyk, A.; Boens, N.; Meuwis, K.; Ameloot, M. *Anal. Biochem.* **1997**, *245*, 28−37.
(11) Kuipers, O. P.; Vincent, M.; Brochon, J. C.; Verheij, H. M.; De Haas, G. H.; Gallay, J. *Biochemistry* **1991**, *30*, 8771−8785.
(12) Boens, N.; Janssens, L. D.; De Schryver, F. C. *Biophys. Chem.* **1989**, *33*, 77−90.
(13) Marquardt, D. W. *J. Soc. Ind. Appl. Math.* **1963**, *11*, 431−441.
(14) Van den Zegel, M.; Boens, N.; Daems, D.; De Schryver, F. C. *Chem. Phys.* **1986**, *101*, 311−335.
(15) Janssens, L. D.; Boens, N.; Ameloot, M.; De Schryver, F. C. *J. Phys. Chem.* **1990**, *94*, 3564−3576.
(16) Meuwis, K.; Depuydt, G.; Boens, N.; De Schryver, F. C. *Chem. Phys. Lett.* **1995**, *246*, 641−648.
(17) Martin, M. M.; Plaza, P.; Meyer, Y. H.; Badaoui, F.; Bourson, J.; Lefèvre J.-P.; Valeur B. *J. Phys. Chem.* **1996**, *100*, 6879−6888.
(18) Martin, M. M.; Plaza, P.; Dai Hung, N.; Meyer, Y. H.; Bourson, J.; Valeur B. *Chem. Phys. Lett.* **1993**, *202*, 425−430.
(19) Mathevet, R.; Jonusauskas, G.; Rullière, C.; Létard, J.-F.; Lapouyade, R. *J. Phys. Chem.* **1995**, *99*, 15709−15713.
(20) Meuwis, K.; Boens, N.; De Schryver, F. C.; Gallay, J.; Vincent, M. *Biophys. J.* **1995**, *65*, 2469−2473.